Journal of Physics: Condensed Matter

PAPER

Real time scissor correction in TD-DFT

IOP Publishing

Journal of Physics: Condensed Matter

J. Phys.: Condens. Matter **31** (2019) 214002 (9pp)

https://doi.org/10.1088/1361-648X/ab048a

Real time scissor correction in TD-DFT

C-Y Wang[1], P Elliott[1,3], S Sharma[2] and J K Dewhurst[1]

[1] Max Planck Institute of Microstructure Physics, Weinberg 2, D-06120 Halle, Germany
[2] Max-Born Institute for Nonlinear Optics and Short Pulse Spectroscopy, Max-Born-Strasse 2A, D-12489 Berlin, Germany

E-mail: peter.elliott@mpi-halle.mpg.de

Received 1 November 2018, revised 17 January 2019
Accepted for publication 5 February 2019
Published 19 March 2019

Abstract

We demonstrate how the scissor correction to the optical band gap, common in linear-response time-dependent density functional theory (TD-DFT), may be extended to the domain of real-time TD-DFT. This requires modifying both the eigenvalues and momentum matrix elements of the underlying basis set. It provides a simple and computationally economical approach for calculating accurate electron dynamics in solids. We demonstrate the importance of this correction for prototypical semiconductors, diamond and silicon, where the energy absorption in both the linear and non-linear regimes is examined. We also show that for a particular system, ZnSe, using the adiabatic local density approximation together with a scissor correction can be advantageous over other approximations, as the underlying quasi-particle band structure is more accurate.

Keywords: TD-DFT, response function, real-time dynamics, scissor correction, optics, method development, DFT

(Some figures may appear in colour only in the online journal)

1. Introduction

The electron dynamics induced by applying ultra-short and intense laser pulses has been of great interest recently [1–7]. In this regime (of fast timescales and large electromagnetic fields) systems responds in non-linear manner leading to several novel and interesting phenomena such as high harmonic generation [8] and dropleton formation [9]. Controlling these processes is an outstanding challenge for Physics and would be of great technological importance. In order to understand the underlying physics of this non-linear charge dynamics and to be able to predict future technology it is essential that we be able to accurately simulate intense light-matter interaction theoretically.

However, as the dynamics of electrons is inherently quantum mechanical in nature (especially in this regime), modeling and simulating these systems is a difficult problem. Moreover, the situation is further complicated for materials where many-body physics and collective excitations must also be correctly included. Hence, it is only in the last few years [3, 10–21] that *ab initio* calculations have been performed for periodic systems.

Time dependent density functional theory (TD-DFT) is the natural candidate to use in this situation. By transforming the problem to the Kohn–Sham (KS) system of non-interacting fermions, realistic simulations become computationally tractable. The electron–electron interaction is then accounted by the exchange-correlation (XC) potential which must be approximated. The standard choice for this is the adiabatic approximation, which utilizes XC functionals from ground-state DFT. TD-DFT thus builds upon the enormous success which DFT has enjoyed in the past few decades [22–24] and has proved successful for both linear response calculations [24] and real-time dynamics [25–27] simulations.

However, using an adiabatic approximation also means we inherit all the problems from the underlying ground-state functional. The most well-known of these is the so-called band gap problem, whereby the KS band gap is typically much smaller than the quasi-particle gap [28, 29]. In TD-DFT, this error manifests itself as an underestimation of the optical absorption edge. This has a drastic effect on the predicted dynamics, for example the material will respond very differently if pumped with laser frequency greater or less than the gap. In the linear-response regime, a simple fix is to apply a scissor-operator which rigidly shifts the conduction band energies in order to correct the optical absorption gap [30]. However for real-time

[3] Author to whom any correspondence should be addressed.

dynamics, this problem has been tackled by using more computationally demanding XC functionals like meta-GGAs, e.g mBJ [31], or Hybrids, e.g. HSE [32].

In this work we extend the concept of the scissor correction to the real-time domain; allowing us to more accurately simulate the dynamics of materials without any extra computational cost. By developing an easy-to-implement fix to the optical band gap problem, we can then utilize XC functionals which otherwise would be ruled out. For example, we will show that the underlying band structure of ZnSe is better described by LDA than by mBJ, but due to LDA underestimating the gap by 1.36 eV, it would be unsuitable for predicting real-time dynamics. Using simpler functionals combined with the real-time scissor correction will allow larger and more sophisticated calculations to be performed.

2. Background theory

2.1. TD-DFT

Time-dependent density functional theory (TD-DFT) is an exact method for calculating the quantum-mechanical dynamics of interacting electrons. The Runge–Gross theorem [33] establishes the uniqueness of the mapping between density and potential, thereby making all observables functionals of the time-dependent density. The theorem also allows the formulation of the KS system, which consists of non-interacting fermions propagating in an effective potential such that it reproduces the density of the interacting electrons. The TD-KS equations read:

$$\mathrm{i}\frac{\partial}{\partial t}\phi_j(\mathbf{r},t) = \left[\frac{1}{2}\left(-\mathrm{i}\boldsymbol{\nabla} - \frac{1}{c}\mathbf{A}(t)\right)^2 + V_{\mathrm{KS}}(\mathbf{r},t)\right]\phi_j(\mathbf{r},t), \tag{1}$$

where atomic units are used throughout, unless otherwise stated. The time-dependent density is

$$n(\mathbf{r},t) = \sum_{j=1}^{N}|\phi_j(\mathbf{r},t)|^2 \tag{2}$$

where $\phi_j(\mathbf{r},t)$ are the Kohn–Sham orbitals, and N is the number of electrons (assuming the initial-state is the ground-state consisting of N fully occupied orbitals).

The Kohn–Sham effective potential is commonly decomposed into:

$$V_{\mathrm{KS}}(\mathbf{r},t) = V_{\mathrm{ext}}(\mathbf{r}) + V_{\mathrm{H}}[n](\mathbf{r},t) + V_{\mathrm{XC}}[n,\Psi_0,\Phi_0](\mathbf{r},t) \tag{3}$$

where $V_{\mathrm{ext}}(\mathbf{r})$, is the external potential containing the electron–ion interaction, $V_{\mathrm{H}}(\mathbf{r},t)$, the Hartree potential describing classical electrostatic interaction, and $V_{\mathrm{XC}}(\mathbf{r},t)$, the exchange-correlation potential. An applied laser pulse is treated in the velocity gauge by the vector potential, $\mathbf{A}(t)$ such that

$$\mathbf{E}(t) = -\frac{1}{c}\frac{\partial\mathbf{A}(t)}{\partial t}. \tag{4}$$

This corresponds to making the dipole approximation for the electric field, $\mathbf{E}(t)$; the electric field is treated as a purely time dependent vector-field which is spatially constant.

The XC potential is formally a functional of the entire history of the density, as well as the initial interacting and non-interacting wave functions Ψ_0 and Φ_0. In a practical TD-DFT calculation, this must be approximated. Commonly a XC functional from ground-state DFT is used with the instantaneous density, this is known as adiabatic approximation.

2.2. Linear response in TD-DFT

The optical absorption spectra, given by the imaginary part of the dielectric function, $\varepsilon(\omega)$, can be calculated from the conductivity tensor, $\sigma(\omega)$, using the relation:

$$\varepsilon(\omega) = 1 + \frac{4\pi\mathrm{i}\sigma(\omega)}{\omega}. \tag{5}$$

The conductivity is defined by the response of the current, $\mathbf{J}(\omega)$, to the applied electric field, $\mathbf{E}(\omega)$:

$$\mathbf{J}(\omega) = \sigma(\omega)\mathbf{E}(\omega). \tag{6}$$

In a real-time TD-DFT simulation, the TD-KS equations, equation (1), are propagated and the time-dependent current is calculated from the KS orbitals. The conductivity can then be found from the Fourier transform of $\mathbf{J}(t)$ and $\mathbf{E}(t)$. The average current per unit cell, $\mathbf{J}(t)$, is calculated via the momentum matrix:

$$\mathbf{J}(t) = \sum_j\sum_{\alpha\beta} c^*_{\alpha j}(t)c_{\beta j}(t)\mathbf{P}_{\alpha\beta} \tag{7}$$

where j labels the occupied TD-KS orbital, which can be expanded in the basis of GS KS states, i.e.

$$\phi_j(\mathbf{r},t) = \sum_\alpha c_{\alpha j}(t)\varphi_\alpha(\mathbf{r}) \tag{8}$$

where

$$\hat{H}^0_{\mathrm{KS}}|\varphi_\alpha\rangle = \epsilon_\alpha|\varphi_\alpha\rangle \tag{9}$$

and H^0_{KS} is the GS DFT KS Hamiltonian. The momentum matrix elements between these GS orbital can then be calculated:

$$\mathbf{P}_{\alpha\beta} = \langle\varphi_\alpha(\mathbf{r})| - \mathrm{i}\nabla|\varphi_\beta(\mathbf{r})\rangle. \tag{10}$$

A convenient choice for calculating the linear response of periodic systems is to use the vector potential

$$A(t) = -c\kappa\theta(t) \tag{11}$$

corresponding to an electric field of $E(t) = \kappa\delta(t)$ where $\theta(t)$ is heaviside step function. The Fourier transform of this electric field is simply a constant, meaning we excite at all frequencies, and drastically simplify equation (6). The parameter κ can either be chosen sufficiently small or the response can expanded to first order as a function of κ.

Alternatively, the dielectric function can be calculated in the linear-response regime using:

$$\varepsilon^{-1}(\omega) = 1 + v\chi(\omega) \tag{12}$$

where v is the bare Coulomb interaction and $\chi(\omega)$ is the linear-response function of the interacting system. It is connected to the KS system via the Dyson-like equation:

$$\chi = \chi_0 + \chi_0(v + f_{\rm XC})\chi \tag{13}$$

in compact notation. The XC kernel, $f_{\rm XC}$, is the functional derivative of $V_{\rm XC}$ with respect to the density. The KS linear response is known from first-order perturbation theory as

$$\chi_0(\mathbf{r},\mathbf{r}',\omega) = \lim_{\eta\to 0}\sum_j\sum_k (n_k - n_j)\frac{\varphi_k^*(\mathbf{r})\varphi_j(\mathbf{r})\varphi_k(\mathbf{r}')\varphi_j^*(\mathbf{r}')}{\omega + (\epsilon_k - \epsilon_m) + \mathrm{i}\eta}. \tag{14}$$

For semi-conducting systems, the KS band gap, given by the energy difference between the highest occupied and lowest unoccupied states, is often much smaller than the quasi-particle band gap. When the absorption spectrum is calculated using equations (12)–(14), this leads to an underestimation of the optical gap. To remedy this problem, the unoccupied conduction band energies can be rigidly shifted to higher energies by the so-called scissor operator [34, 35], often leading to reasonable spectra [30, 36].

2.3. The time-dependent energy functional

Although the Runge–Gross theorem states that all observables are unique functionals of the density, in many cases the exact functional dependence is not known. Thus, we require additional approximations for such observables. One such observable is the time dependent energy, for which a reasonable approximate form reads:

$$E[n](t) = \sum_{j=1}^{N} -\frac{1}{2}\langle\phi_j|\nabla^2|\phi_j\rangle + \int V_{\rm ext}(\mathbf{r},t)n(\mathbf{r},t)\mathrm{d}^3r + U[n(t)] + E_{\rm XC}[n(t)] \tag{15}$$

where $U[n]$ is the Hartree electrostatic energy and $E_{\rm XC}[n]$ is the XC energy corresponding to the ground-state XC potential used within the adiabatic approximation. It is known that this energy is conserved in the absence of external perturbations [37, 38] and will be exact in the adiabatic limit. By comparing this energy before and after an applied laser pulse, one can estimate the energy absorbed by the system.

2.4. Real-time propagation

There are many propagation schemes [39] for the TD-KS equation (equation (1)), such as Crank–Nicolson, split-operator, Runge–Kutta, etc. In the ELK electronic structure code [40], the following algorithm is used:

(i) The TD-KS orbital is written in the basis of GS orbitals, as was seen in equation (8):

$$\phi_j(\mathbf{r},t) = \sum_\alpha c_{\alpha j}(t)\varphi_\alpha(\mathbf{r}) \tag{16}$$

(ii) Potential $V_{\rm KS}(\mathbf{r},t)$ is calculated from $n(\mathbf{r},t)$ (this determines $\hat{H}_{\rm KS}(t)$).

(iii) The Hamiltonian is then diagonalized in the GS orbital basis

$$\sum_\gamma H^t_{\beta\gamma}a_{\gamma\alpha} = \tilde{\epsilon}_\alpha a_{\beta\alpha} \tag{17}$$

where

$$\begin{aligned} H^t_{\alpha\beta} &= \langle\varphi_\alpha \mid \hat{H}_{\rm KS}(t) \mid \varphi_\beta\rangle \\ &= \epsilon_\alpha\delta_{\alpha\beta} + \langle\varphi_\alpha \mid \delta\hat{V}_{\rm KS}(t) \mid \varphi_\beta\rangle \end{aligned} \tag{18}$$

and

$$\delta\hat{V}_{\rm KS}(t) = \hat{H}_{\rm KS}(t) - \hat{H}^0_{\rm KS}. \tag{19}$$

(iv) Each orbital $\phi_j(\mathbf{r},t)$ is projected into this instantaneous eigenstate basis and time evolved to the next time step:

$$c_{\alpha j}(t+\Delta t) = \sum_{\beta\gamma} a^*_{\gamma\beta}c_{\gamma j}(t)a_{\alpha\beta}\mathrm{e}^{-\mathrm{i}\tilde{\epsilon}_\beta\Delta t}. \tag{20}$$

Further details of this algorithm can be found in [41].

3. The scissor correction in real-time TD-DFT

The real-time (RT) scissor correction is done in two steps. First the conduction band GS orbital energies are shifted by Δ

$$\begin{cases} \epsilon_\alpha = \epsilon_\alpha & \epsilon_\alpha \leqslant \epsilon_{\rm F} \\ \epsilon_\alpha = \epsilon_\alpha + \Delta & \epsilon_\alpha > \epsilon_{\rm F} \end{cases} \tag{21}$$

where $\epsilon_{\rm F}$ is the Fermi energy. These energies enter the time-propagation via equation (18). Secondly, the momentum matrices used to calculate the current and the coupling to the $\mathbf{A}$ field are scaled by a factor $(\epsilon_{\alpha\beta} + \Delta)/\epsilon_{\alpha\beta}$:

$$\tilde{\mathbf{P}}_{\alpha\beta} = \frac{\epsilon_{\alpha\beta}+\Delta}{\epsilon_{\alpha\beta}}\mathbf{P}_{\alpha\beta}. \tag{22}$$

Thus this scaling factor would directly affect the value of $\mathbf{J}(t)$, see equation (7).

In [30], it was shown that the XC kernel of linear-response TD-DFT can be separated into two terms. The first corrects the band gap, while the second is responsible for capturing the excitonic physics. If this approach is extended to the real-time case, then the effect of the first term can be reproduced using the scissor correction outlined above. Thus Δ should be chosen to correct the KS gap to the fundamental gap. This can be done using a one-time higher level DFT GKS calculation, e.g. using a meta-GGA/hybrid functional, or via many-body perturbation theory, e.g. using the GW approximation (i.e. $\Delta = \epsilon_{\rm g}^{\rm GW} - \epsilon_{\rm g}^{\rm KS}$). Alternatively Δ may be set empirically using the experimental absorption spectra.

3.1. Computational details

All calculations were performing using the all-electron full-potential linearised-augmented-plane-wave (LAPW) elk code [40]. In all cases, the experimental lattice parameters [42] were used: 3.57 Å for diamond, 5.43 Å for silicon and 5.67 Å for zinc selenide. A shifted $\mathbf{k}$-point grid of at least $10 \times 10 \times 10$ was used. For real-time propagation, a time step of 0.0024 femtosecond was used. In order to acquire reasonable linear

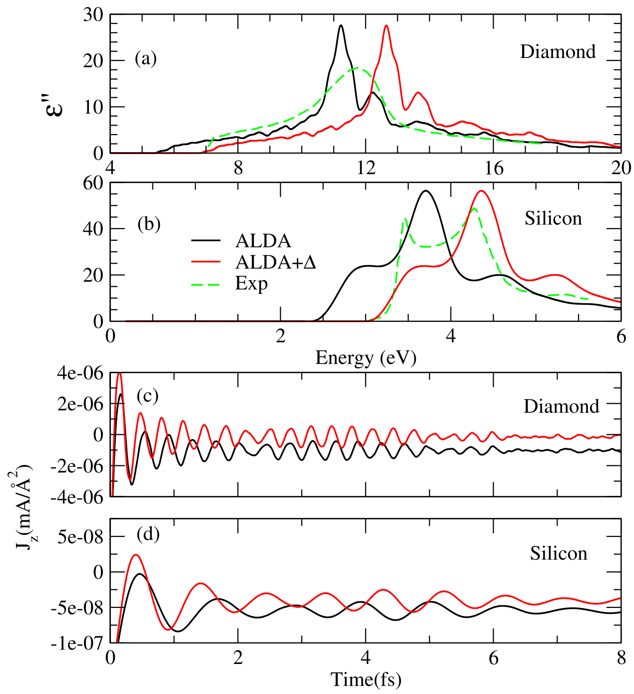

Figure 1. The spectrum calculated from real time TD-DFT simulations for the dielectric function ($\epsilon(\omega) = \epsilon'(\omega) + \mathrm{i}\epsilon''(\omega)$) of diamond and silicon with ALDA and scissor corrected ALDA for (a) diamond and (b) silicon. The unit-cell averaged current in diamond and silicon induced by the perturbation is shown in (c) and (d).

response spectra from real-time propagation, a total simulation time, T, of 27.8 femtoseconds was required. Following [25], a third-order polynomial in the form of

$$f(t) = 1 - 3\left(\frac{t}{T}\right)^2 + 2\left(\frac{t}{T}\right)^3 \tag{23}$$

is applied to current $\mathbf{J}(t)$ in order to eliminate high frequency oscillations in the Fourier transform. The real time scissor shifts, Δ, were set empirically to correct the optical absorption gap: 0.86 eV for Si, 1.42 eV for C, and 1.36 eV for ZnSe. Simlar values for Δ would be found by the direct band gap based on GW calculation [43–45].

4. Results and discussion

4.1. Linear regime

Figures 1(a) and (b) show the absorption spectra of diamond and silicon calculated using the adiabatic local density approximation (ALDA) with and without the scissor correction (labeled ALDA+ Δ and ALDA). In order to calculate the dielectric function the unit-cell averaged current was calculated and the spectra extracted via equations (5) and (6). These currents are shown in figures 1(c) and (d). As expected the scissors corrected absorption spectra is exactly the same as the uncorrected spectra but rigidly shift to higher energy by amount Δ. When comparing this data to experiments we find that for silicon, the ALDA+ Δ spectrum correctly reproduces the absorption peak at 4.4 eV. The peak around 3 eV in the experimental data is due to excitons and is strongly underestimated in the TD-DFT results. This is due to the ALDA kernel not including electron and hole interactions, and thus misses excitonic effects. For diamond the uncorrected spectra appears to be in better agreement with experimental data. However, this is highly misleading; in diamond the excitonic effects shift the spectra to lower energies by the same amount [46, 47] as the underestimation of the Kohn–Sham band gap. Thus the two effects cancel giving the appearance of a better agreement. Thus uncorrected ALDA leads to correct position of absorption peak for the wrong reasons.

In order to demonstrate the importance of this correction in figure 2 we plot the absorbed energy as a function of time for diamond and silicon irradiated with laser pulses of two different frequencies: (1) a frequency below the true optical gap, but above the LDA gap (2.72 eV for silicon, 5.61 eV for diamond), and (2) a frequency slightly above the true direct gap (3.58 eV for silicon, 7.33 eV for diamond). For these calculations, we use the following vector potential:

$$\mathbf{A}(t) = \mathbf{A}_0 \frac{\mathrm{e}^{-(t-t_0)^2/2\sigma_g^2}}{\sigma_g\sqrt{2\pi}} \sin(\omega(t-t_0)) \tag{24}$$

which corresponds to a laser pulse of frequency ω, with a Gaussian envelope of width σ_g centered at time t_0. The incident intensity is controlled by the amplitude, A_0. In this case we choose amplitudes corresponding to peak intensities of 10^{11} W cm^{-2} for silicon and 10^{12} W cm^{-2} for diamond. The variance σ_g is chosen to give a FWHM of 6.29 fs.

Since for these intensities the linear order term in the response function is dominating, we expect to see little-to-no absorption for frequencies below the band gap (note, the transient behavior of the energy during the pulse was explored in Schultze *et al* [48]). However, we find in figures 2(a) and (c) that ALDA vastly overestimates the absorbed energy. The scissor corrected calculation also shows a non-zero absorption for these frequencies due to the contribution of higher order effects even at these small intensities. Pumping the system with pulses above the direct band gap of the material, we see in figures 2(b) and (d), that both ALDA and ALDA+Δ now show absorption, however ALDA shows much larger absorption.

This behavior can be understood by the cartoon in figure 3, which shows a simplified representation of the underlying band structure of ALDA and ALDA+Δ. Consider what will happen if we were to pump with the frequency labeled ω in figure 3(a), which is less than the true gap. In this case we should not excite any electrons from the valence to the conduction band, and should not absorb any energy. If we now compare how ALDA and ALDA+Δ will behave for this scenario, we find very different results. With this frequency we can reach the LDA conduction band, hence ALDA will erroneously absorb energy, while ALDA+Δ will behave correctly. If we instead pump with the frequency ω' illustrated in figure 3(b), we can now reach the respective conduction bands for both cases, meaning both will absorb. However, as ALDA will have a higher density of available states in which to excite, hence it overestimates the absorption in this case.

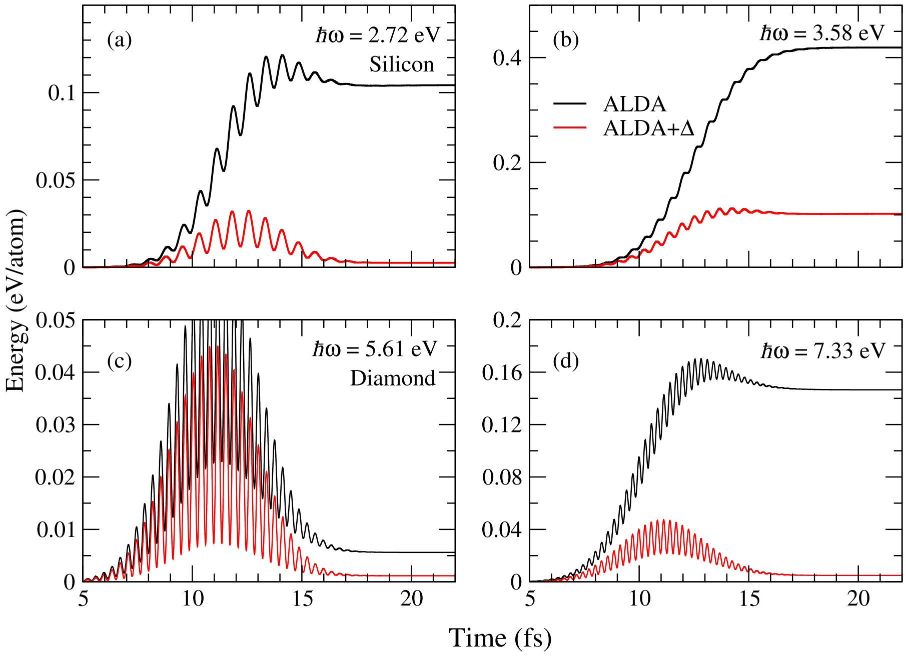

Figure 2. The energy absorbed by silicon (a), (b) and diamond (c), (d) due to applied laser pulses in linear response regime with frequencies below (a), (c) and above (b), (d) the respective optical gaps.

4.2. Nonlinear regime

We now go beyond the linear regime to study the response of semiconductors to strong laser pulses. This non-linear regime, where novel and interesting processes such as multi-photon absorption occur, is increasingly probed by experiment. Here the dependence on the laser pulse intensity is determined by underlying band structure, thus it is vitally important to correctly describe the correct positions of these bands, in order to perform accurate *ab initio* simulations of such systems.

The dependence of the absorbed energy as a function of laser peak intensity is shown in figure 4 for silicon and diamond. The frequency of the laser is chosen to be half of the LDA gap ($\omega = 1.36$ eV for Si and $\omega = 2.80$ eV for diamond), so that there is little linear response in both the ALDA and ALDA + Δ cases. As the laser intensity increases, the probability of absorbing multiple photons increases, signifying the onset of non-linear behavior. Here we find that ALDA predicts a much lower threshold for non-linear behavior for both Si and diamond. The scissor corrected ALDA behaves as expected, and is at least an order of magnitude higher than ALDA. Such a large difference between the two cases shows the importance of the scissor correction for obtaining the threshold for nonlinear effect. For this particular choice of frequency, diamond requires a much stronger laser pulse to reach the non-linear regime due to the difference in the percentage error of the LDA gap error and the difference in the conduction band structure.

4.3. Comparison to meta-GGA functionals

In this section, we compare our ALDA+Δ correction to an alternative approach to the band gap problem. The modified Becke–Johnson (mBJ) potential [31] is known to provide

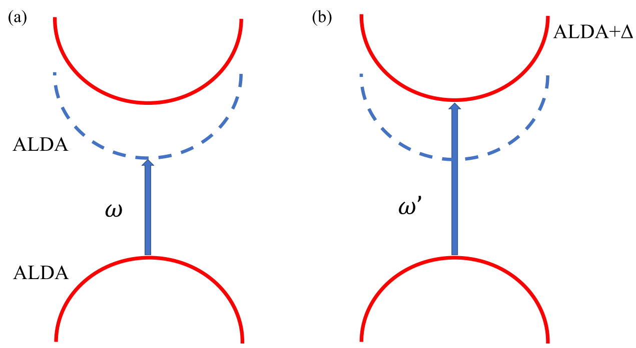

Figure 3. Schematic showing how LDA and scissor-corrected LDA band structure leads to overestimation of the ALDA absorbed energy.

KS band gaps closer to the quasi-particle band gap. Hence, it has been proposed as a solution to the optical gap problem in TD-DFT [49]. Indeed a recent study [50] has shown that the absorption spectra for silicon calculated from a real-time TD-DFT calculation using the mBJ potential agrees well with experiment. However GS calculations have shown that while mBJ can predict reasonable band gaps, the bandwidths are often underestimated [51, 52]. This can be seen in s, p band semiconductors such as MgO, as well as d-band materials such as ZnSe. In the following, we will focus on the semiconductor ZnSe, which has a direct gap of 2.82 eV [53], to see how this band-narrowing in the mBJ band structure affects the absorption spectrum. Note, we use $\mathrm{mBJ_{opt}}$ to refer to the mBJ functional tuned to give $\epsilon_g^{KS} = \epsilon_g^{Exp}$.

In figure 5 we compare the band structure of ZnSe from $\mathrm{mBJ_{opt}}$ and scissor-corrected LDA calculations to the higher-level GW quasi-particle band structure from [45]. By design, both LDA+Δ and $\mathrm{mBJ_{opt}}$ give the correct direct band gap at the Γ point. Following the bands throughout the Brillouin zone, we see that $\mathrm{mBJ_{opt}}$ has squeezed the width of both the

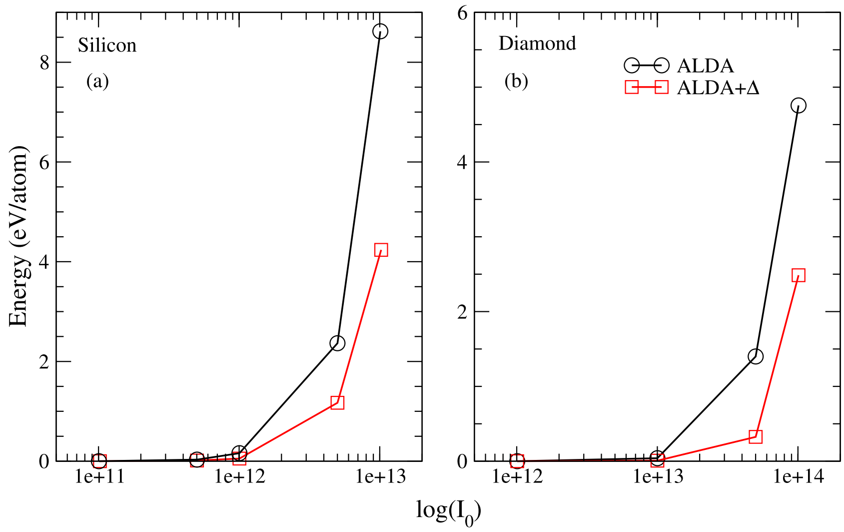

Figure 4. The energy absorbed by (a) silicon and (b) diamond after a short laser pulse as a function of the peak intensity (plotted on a log scale). The frequency of laser pulse is chosen to be half the respective LDA band gap.

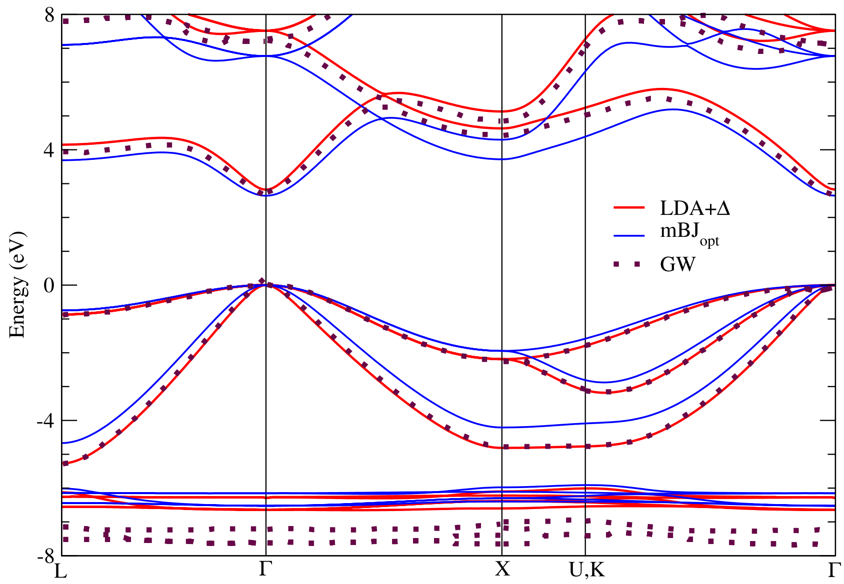

Figure 5. Band structures of ZnSe from calculations of scissor corrected LDA, modified Becke–Johnson potential, and GW MBPT. Reprinted figure with permission from [45], copyright 2002 by the American Physical Society.

valence and conduction bands. This can be best seen at the X point where the valence band at -4 eV (relative to the Fermi energy) is 1 eV higher than the GW band, while the lowest conduction band is 1 eV too low. The LDA+Δ bands are in much better agreement with the GW calculations.

The cumulative effect of the incorrect mBJ_{opt} band structure can be seen in the optical absorption spectrum plotted in figure 6, where we performed real-time linear response calculations for both ALDA+Δ and mBJ_{opt}. We compare to the experimental results from [54], where three prominent peaks at 4.75 eV, 6.40 eV, and 8.25 eV can be resolved. For each of these peaks, the mBJ_{opt} results are 0.5 eV too low. This is consistent with the bandwidth narrowing we observed in figure 5. In contrast, the position of these peaks predicted by ALDA+Δ is in better agreement with experimental. Both the first and third peaks are correct, while the second peak is 0.3 eV too high.

Finally, we compare the absorbed energy predicted by ALDA+Δ and mBJ_{opt} for two laser pulses with frequencies 6.07 eV and 6.67 eV respectively as shown in figure 7. In the first case, mBJ_{opt} predicts a more excited final state than ALDA+ Δ, while the situation is reversed for the second pulse. This demonstrates how important the choice of functional is when simulating laser induced dynamics, as they can give even opposite results. In figure 6 we saw that ALDA+Δ gave a better description of the absorption spectrum of ZnSe, it follows that it will be a better choice when investigating real-time dynamics. Particularly if quantitative comparison with experimental work is desired.

While we focused on ZnSe, the problems mBJ has in describing the band structure of *d*-electrons are known for a number of materials [51]. For such cases, we have seen that this leads to errors in the TD-DFT dynamics and thus using ALDA + Δ will be a better choice, for these materials.

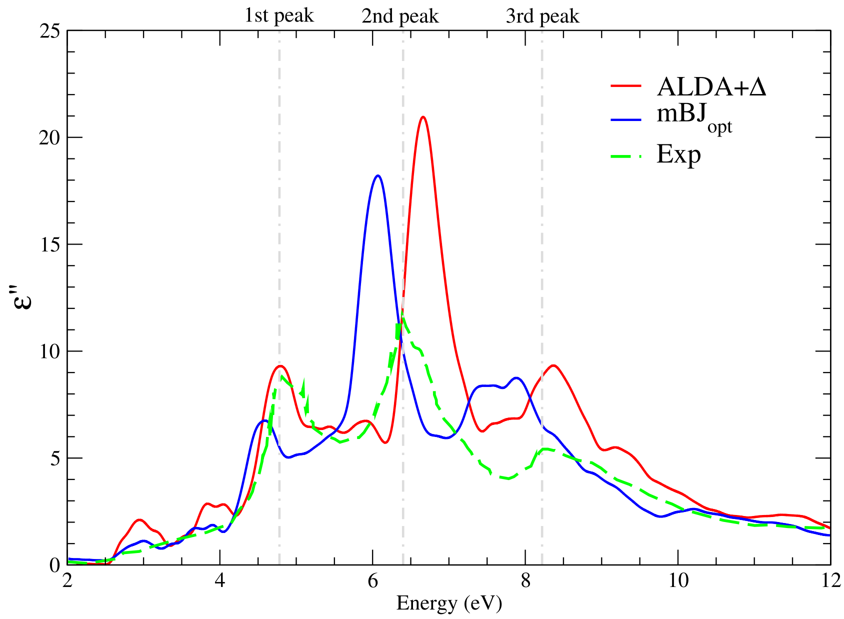

Figure 6. The $\epsilon''(\omega)$ of ZnSe from real-time linear response calculations using scissor corrected ALDA and the optimized modified Beche–Johnson potential mBJ_{opt}, compared to the experimental data from [54].

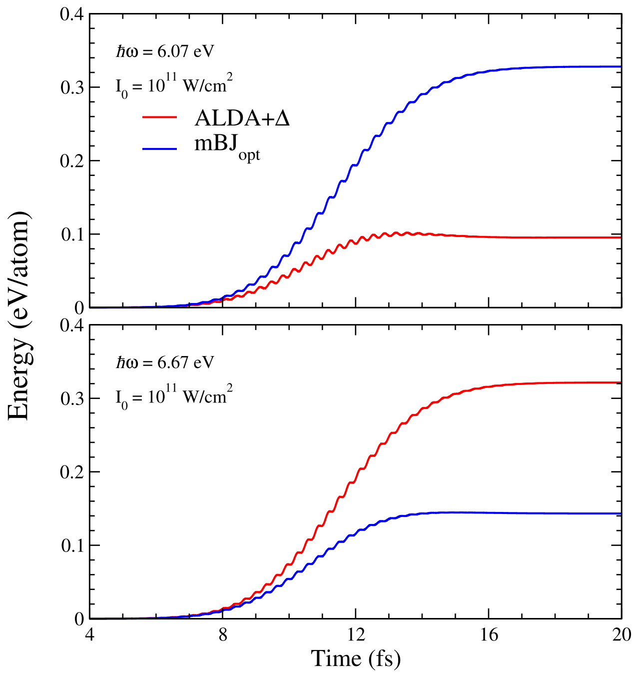

Figure 7. Energy absorbed by ZnSe following applied laser pulses of frequency 6.07 eV (upper panel) and 6.67 eV and peak intensity 10^{11} W cm^{-2}.

5. Summary

To summarize, in this paper we have implemented a computationally simple scheme to rectify the band gap problem in real-time TD-DFT simulations. We have demonstrated why such a fix is necessary. In particular, when pumping below the optical band gap, where uncorrected ALDA behaves qualitatively incorrectly. We have also investigated how the real-time scissor correction is essential for describing non-linear dynamics such as multi-photon absorption. This allows the full power of TD-DFT to be easily utilized in the emerging field of ultra-fast, ultra-strong, laser pulses. We note that in the linear-response regime, XC kernels which can predict excitons, also require a scissor correction. Thus it is likely that the real-time scissor correction is a necessary development along with XC potentials which can correctly describe excitons in real time.

The real-time scissor correction presented here consists of two changes to the underlying orbitals: (1) the eigenvalues above the Fermi level are shifted by Δ, and (2) the momentum matrix elements are re-scaled. The value of Δ may be found *ab initio*, from a one-time higher level calculation (e.g. mBJ or HSE or hybrid functionals within DFT or GW method). While we applied this procedure to all states, it may be easily modified to act on individual bands. This would be useful in cases where the DFT band structure is reasonable except for the positioning of particular bands such as deeper, localized, states, and is not necessarily restricted to insulating or semiconducting systems. One might also apply a k-dependent scissor shift to correct the band structure at particular k-points. Another possible modification is to use a time-dependent scissor operator to help account for changes in the band structure during non-linear dynamics. This method may also be applied to similar methods to TD-DFT, e.g. time-dependent current density functional theory, in cases where the optical band gap is also underestimated.

Lastly we demonstrated how the real-time scissor method is a more suitable choice for describing the dynamics of ZnSe compared to the meta-GGA mBJ functional. While both approaches correct the optical band gap as required, we found the mBJ optical absorption spectra to be worse than ALDA+ Δ. This is due to errors in the underlying band structure, where mBJ is known to incorrectly narrow the bandwidth of some bands. Thus, it is better to use the real-time scissor correction to calculate the dynamics of ZnSe and similar materials.

Acknowledgments

SS acknowledges support from DFG through TRR 227.

ORCID iDs

C-Y Wang https://orcid.org/0000-0002-3191-4273

References

[1] Beaurepaire E, Merle J-C, Daunois A and Bigot J-Y 1996 Ultrafast spin dynamics in ferromagnetic nickel *Phys. Rev. Lett.* **76** 4250

[2] Schiffrin A *et al* 2013 Optical-field-induced current in dielectrics *Nature* **493** 70

[3] Yabana K, Sugiyama T, Shinohara Y, Otobe T and Bertsch G F 2012 Time-dependent density functional theory for strong electromagnetic fields in crystalline solids *Phys. Rev.* B **85** 045134

[4] Goulielmakis E *et al* 2010 Real-time observation of valence electron motion *Nature* **466** 739

[5] Rozzi C A *et al* 2013 Quantum coherence controls the charge separation in a prototypical artificial light-harvesting system *Nat. Commun.* **4** 1602

[6] Le Guyader L *et al* 2012 Demonstration of laser induced magnetization reversal in GdFeCo nanostructures *Appl. Phys. Lett.* **101** 022410

[7] Eschenlohr A, Battiato M, Maldonado P, Pontius N, Kachel T, Holldack K, Mitzner R, Föhlisch A, Oppeneer P M and Stamm C 2013 Ultrafast spin transport as key to femtosecond demagnetization *Nat. Mater.* **12** 332

[8] Li W, Zhou X, Lock R, Patchkovskii S, Stolow A, Kapteyn H C and Murnane M M 2008 Time-resolved dynamics in N_2O_4 probed using high harmonic generation *Science* **322** 1207

[9] Almand-Hunter A E, Li H, Cundiff S T, Mootz M, Kira M and Koch S W 2014 Quantum droplets of electrons and holes *Nature* **506** 471

[10] Grüning M and Attaccalite C 2014 Second harmonic generation in h-BN and MoS_2 monolayers: role of electron–hole interaction *Phys. Rev.* B **89** 081102

[11] Karlsson D, Privitera A and Verdozzi C 2011 Time-dependent density-functional theory meets dynamical mean-field theory: real-time dynamics for the 3d Hubbard model *Phys. Rev. Lett.* **106** 116401

[12] Attaccalite C, Grüning M and Marini A 2011 Real-time approach to the optical properties of solids and nanostructures: time-dependent bethe-salpeter equation *Phys. Rev.* B **84** 245110

[13] Stamenova M, Simoni J and Sanvito S 2016 Role of spin–orbit interaction in the ultrafast demagnetization of small iron clusters *Phys. Rev.* B **94** 014423

[14] Krieger K, Dewhurst J K, Elliott P, Sharma S and Gross E K U 2015 Laser-induced demagnetization at ultrashort time scales: predictions of TDDFT *J. Chem. Theory Comput.* **11** 4870–4

[15] Elliott P, Müller T, Dewhurst J K, Sharma S and Gross E K U 2016 Ultrafast laser induced local magnetization dynamics in Heusler compounds *Sci. Rep.* **6** 38911

[16] Krieger K, Elliott P, Müller T, Singh N, Dewhurst J K, Gross E K U and Sharma S 2017 Ultrafast demagnetization in bulk versus thin films: an *ab initio* study *J. Phys.: Condens. Matter* **29** 224001

[17] Dewhurst J K, Elliott P, Shallcross S, Gross E K U and Sharma S 2018 Laser-induced intersite spin transfer *Nano Lett.* **18** 1842–8

[18] Elliott P, Stamenova M, Simoni J, Sharma S, Sanvito S and Gross E K U 2018 Time-dependent density functional theory for spin dynamics *Handbook of Materials Modeling: Methods: Theory and Modeling* ed W Andreoni and S Yip (Cham: Springer) pp 1–26

[19] Attar A R, Bhattacherjee A, Pemmaraju C D, Schnorr K, Closser K D, Prendergast D and Leone S R 2017 Femtosecond x-ray spectroscopy of an electrocyclic ring-opening reaction *Science* **356** 54–9

[20] Floss I, Lemell C, Wachter G, Smejkal V, Sato S A, Tong X-M, Yabana K and Burgdörfer J 2018 *Ab initio* multiscale simulation of high-order harmonic generation in solids *Phys. Rev.* A **97** 011401

[21] Dewhurst J K, Shallcross S, Gross E K U and Sharma S 2018 Substrate-controlled ultrafast spin injection and demagnetization *Phys. Rev. Appl.* **10** 044065

[22] Marques M A L and Gross E K U 2004 Time-dependent density functional theory *Annu. Rev. Phys. Chem.* **55** 427

[23] Burke K, Werschnik J and Gross E K U 2005 Time-dependent density functional theory: past, present, and future *J. Chem. Phys.* **123** 062206

[24] Casida M E and Huix-Rotllant M 2012 Progress in time-dependent density-functional theory *Annu. Rev. Phys. Chem.* **63** 287

[25] Yabana K, Nakatsukasa T, Iwata J-I and Bertsch G F 2006 Realtime, real space implementation of the linear response timedependent density functional theory *Phys. Status Solidi* b **243** 1121

[26] Shokeen V, Sanchez Piaia M, Bigot J-Y, Müller T, Elliott P, Dewhurst J K, Sharma S and Gross E K U 2017 Spin flips versus spin transport in nonthermal electrons excited by ultrashort optical pulses in transition metals *Phys. Rev. Lett.* **119** 107203

[27] Chen J, Bovensiepen U, Eschenlohr A, Müller T, Elliott P, Gross E K U, Dewhurst J K and Sharma S 2018 Competing spin transfer and dissipation at Co/Cu (0 0 1) interfaces on femtosecond timescales (arXiv:1803.03090)

[28] Sham L J and Schlüter M 1985 Density-functional theory of the band gap *Phys. Rev.* B **32** 3883

[29] Zhu X and Louie S G 1991 Quasiparticle band structure of thirteen semiconductors and insulators *Phys. Rev.* B **43** 14142

[30] Sharma S, Dewhurst J K and Gross E K U 2014 Optical response of extended systems using time-dependent density functional theory *First Principles Approaches to Spectroscopic Properties of Complex Materials* ed C Di Valentin *et al* (New York: Springer) pp 235–57

[31] Tran F and Blaha P 2009 Accurate band gaps of semiconductors and insulators with a semilocal exchange-correlation potential *Phys. Rev. Lett.* **102** 226401

[32] Heyd J, Scuseria G E and Ernzerhof M 2003 Hybrid functionals based on a screened Coulomb potential *J. Chem. Phys.* **118** 8207

[33] Runge E and Gross E K U 1984 Density-functional theory for time-dependent systems *Phys. Rev. Lett.* **52** 997

[34] Levine Z H and Allan D C 1989 Linear optical response in silicon and germanium including self-energy effects *Phys. Rev. Lett.* **63** 1719

[35] Nastos F, Olejnik B, Schwarz K and Sipe J E 2005 Scissors implementation within length-gauge formulations of the frequency-dependent nonlinear optical response of semiconductors *Phys. Rev.* B **72** 045223

[36] Kootstra F, de Boeij P L and Snijders J G 2000 Application of time-dependent density-functional theory to the dielectric function of various nonmetallic crystals *Phys. Rev.* B **62** 7071

[37] Bertsch G F, Iwata J-I, Rubio A and Yabana K 2000 Real-space, real-time method for the dielectric function *Phys. Rev.* B **62** 7998

[38] Mundt M 2007 Orbital functionals in time-dependent density-functional theory *PhD Thesis* University of Bayreuth
[39] Castro A, Appel H, Rozzi C A, Oliveira M, Andrade X, Lorenzen F, Marques M A L, Gross E K U and Rubio A 2006 Octopus: a tool for the application of time-dependent density functional theory *Phys. Status Solidi* b **243** 2465
[40] Dewhurst J K *et al* The Elk Code http://elk.sourceforge.net
[41] Dewhurst J K, Krieger K, Sharma S and Gross E K U 2016 An efficient algorithm for time propagation as applied to linearized augmented plane wave method *Comput. Phys. Commun.* **209** 92
[42] Wyckoff R W G 1963 *Crystal Structures* vol 1, 2nd edn (New York: Interscience)
[43] Hybertsen M S and Louie S G 1985 First-principles theory of quasiparticles: calculation of band gaps in semiconductors and insulators *Phys. Rev. Lett.* **55** 1418
[44] Godby R W, Schlüter M and Sham L J 1988 Self-energy operators and exchange-correlation potentials in semiconductors *Phys. Rev.* B **37** 10159
[45] Luo W, Ismail-Beigi S, Cohen M L and Louie S G 2002 Quasiparticle band structure of ZnS and ZnSe *Phys. Rev.* B **66** 195215
[46] Sharma S, Dewhurst J K, Sanna A and Gross E K U 2011 Bootstrap approximation for the exchange-correlation kernel of time-dependent density-functional theory *Phys. Rev. Lett.* **107** 186401
[47] Sharma S, Dewhurst J K, Shallcross S, Madjarova G K and Gross E K U 2015 Excitons in organics using time-dependent density functional theory: PPV, pentacene, and picene *J. Chem. Theory Comput.* **11** 1710–4
[48] Schultze M *et al* 2013 Controlling dielectrics with the electric field of light *Nature* **493** 75
[49] Sato S A, Yabana K, Shinohara Y, Otobe T, Lee K-M and Bertsch G F 2015 Time-dependent density functional theory of high-intensity short-pulse laser irradiation on insulators *Phys. Rev.* B **92** 205413
[50] Sato S A, Taniguchi Y, Shinohara Y and Yabana K 2015 Nonlinear electronic excitations in crystalline solids using meta-generalized gradient approximation and hybrid functional in time-dependent density functional theory *J. Chem. Phys.* **143** 224116
[51] Singh D J 2010 Electronic structure calculations with the Tran–Blaha modified Becke–Johnson density functional *Phys. Rev.* B **82** 205102
[52] Waroquiers D, Lherbier A, Miglio A, Stankovski M, Poncé S, Oliveira M J T, Giantomassi M, Rignanese G-M and Gonze X 2013 Band widths and gaps from the Tran-Blaha functional: comparison with many-body perturbation theory *Phys. Rev.* B **87** 075121
[53] Venghaus H 1979 Valence-band parameters and *g* factors of cubic zinc selenide derived from free-exciton magnetoreflectance *Phys. Rev.* B **19** 3071
[54] Freeouf J L 1973 Far-ultraviolet reflectance of II–VI compounds and correlation with the Penn–Phillips gap *Phys. Rev.* B **7** 3810